This is an open access article published under a Creative Commons Attribution (CC-BY) License, which permits unrestricted use, distribution and reproduction in any medium, provided the author and source are cited.

THE JOURNAL OF PHYSICAL CHEMISTRY B

Article

pubs.acs.org/JPCB

Dielectric Relaxation of the Ionic Liquid 1-Ethyl-3-methylimidazolium Ethyl Sulfate: Microwave and Far-IR Properties

Nilesh R. Dhumal,[†] Johannes Kiefer,[‡] David Turton,[§] Klaas Wynne,[§] and Hyung J. Kim*[,†,∥,⊥]

[†]Department of Chemistry, Carnegie Mellon University, Pittsburgh, Pennsylvania 15213, United States

[‡]Technische Thermodynamik, Universität Bremen, 28359 Bremen, Germany

[§]School of Chemistry, University of Glasgow, Glasgow G12 8QQ, U.K.

[∥]School of Computational Sciences, Korea Institute for Advanced Study, Seoul 02455, Korea

ABSTRACT: Dielectric relaxation of the ionic liquid, 1-ethyl-3-methylimidazolium ethyl sulfate (EMI^+ETS^-), is studied using molecular dynamics (MD) simulations. The collective dynamics of polarization arising from cations and anions are examined. Characteristics of the rovibrational and translational components of polarization dynamics are analyzed to understand their respective roles in the microwave and terahertz regions of dielectric relaxation. The MD results are compared with the experimental low-frequency spectrum of EMI^+ETS^-, obtained via ultrafast optical Kerr effect (OKE) measurements.

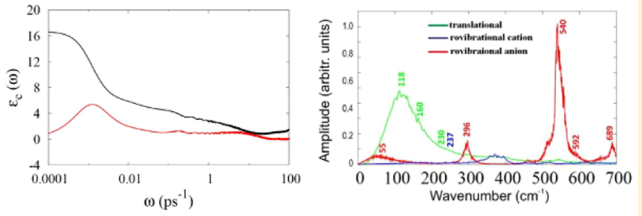

INTRODUCTION

Dielectric relaxation and the related conductivity of a condensed-phase system arise from molecular motions that modulate its local electric dipole moment.[1] Far-IR (FIR) and terahertz spectroscopy offers an excellent experimental tool to probe these motions, both the individual and the collective (inter)molecular motions, subject to the influence of the local structure. Dielectric absorption data obtained by these techniques as well as via microwave spectroscopy have been very useful in theoretical modeling and understanding of the dynamics in polar solvents and ionic solutions.[2−9]

Ionic liquids (ILs) consisting of bulky organic cations paired with organic or inorganic anions are characterized by an anisotropy in the charge distribution and shape. These attributes make ILs an interesting and challenging class of materials to understand their dielectric and related properties, as they have characteristics of both polar liquids and ionic melts. At the molecular level, IL ions have both a net charge and a permanent dipole moment (except for highly symmetric anions such as PF_6^- and BF_4^-). At the dielectric or mesoscopic level, these properties result in significant ion conductivity and dielectric permittivity. According to many simulation studies,[10−15] the collective reorientational and translational motions of the ions make differing contributions to the dielectric relaxation in the gigahertz and terahertz regions. In this respect, spectroscopic measurements in both the microwave and FIR regions would be needed to fully resolve and understand the cation−anion interactions and their dynamics in these Coulomb fluids.[16−18]

The static dielectric constant ε_0, arising from collective ion reorganization via both reorientation and translation in response to an external electric field, ranges between ∼10 and ∼16 for most ILs.[10,16,19−22] Despite their modest ε_0 value,[23] the effective polarity of ILs, which is measured as solvatochromic shifts gauging their capability of solvating dipolar solutes, is comparable to and often in excess of that of highly polar solvents, such as acetonitrile.[24] Interestingly, the ε_0 value of many ILs shows a weaker temperature dependence than for polar solvents. The antagonistic roles played by IL ion translations and reorientations are responsible for this behavior. The former and latter tend to increase and decrease ε_0, respectively, as temperature rises.[15]

In this article, we examine the dielectric relaxation of 1-ethyl-3-methylimidazolium ethyl sulfate (EMI^+ETS^-), one of the first ILs commercially available. Its halide-free synthesis was first studied by Holbrey and co-workers[25] and aspects of reactor design were discussed by Böwing and Jess.[26] Its static dielectric constant is considerably higher than the typical value for many other ILs; the ε_0 value for EMI^+ETS^- was reported to be 27.9 in ref 21. In addition to its use as a green solvent, EMI^+ETS^- has a potential application in chemical separation, in particular, in the separation of azeotropic mixtures.[27] Therefore, extensive attention has been paid to its bulk and interfacial properties.[28−39] Herein, we investigate the dielectric susceptibility of EMI^+ETS^- in the gigahertz and terahertz regions via MD and analyze the respective roles played by translational and reorientational motions of cations and anions. The spectroscopic information extracted from the MD simulations is compared with the dielectric loss spectroscopy results[40] as well as with the low-frequency spectrum obtained from ultrafast optical Kerr effect (OKE) measurements.

Received: January 6, 2017
Revised: March 28, 2017
Published: April 25, 2017

 © 2017 American Chemical Society

DOI: 10.1021/acs.jpcb.7b00160
J. Phys. Chem. B 2017, 121, 4845−4852

THEORY AND METHODS

Dielectric Relaxation and Ion Conductivity. We begin with a brief reprise of the linear response theory for dielectric relaxation (for details, see refs 10 and 14). The electric susceptibility $\chi(\omega)$ is defined as

$$\chi(\omega) = \int_0^\infty \mathrm{d}t\ \mathrm{e}^{\mathrm{i}\omega t}\chi(t)$$
$$\frac{1}{V}\bar{\mathbf{M}}_{\mathrm{tot}}(t) = \int_{-\infty}^{t} \mathrm{d}t'\ \chi(t-t')\ \mathbf{E}(t')$$
$$\mathbf{M}_{\mathrm{tot}} = \sum_{i,\alpha} q_{i,\alpha}\mathbf{r}_{i,\alpha} \tag{1}$$

where $\bar{\mathbf{M}}_{\mathrm{tot}}(t)$ is the average total dipole moment of the system at time t induced by a time-dependent homogeneous electric field $\mathbf{E}(t)$, V is the volume, $q_{i,\alpha}$ and $\mathbf{r}_{i,\alpha}$ are, respectively, the charge and position of the site i of ion α, and the sum is taken over charge sites of all ions. Generalized dielectric constant $\varepsilon(\omega)$ and conductivity $\sigma(\omega)$ are introduced as

$$4\pi\chi(\omega) = \varepsilon'(\omega) + \mathrm{i}\varepsilon''(\omega) - 1 = \mathrm{i}\frac{4\pi}{\omega}[\sigma'(\omega) + \mathrm{i}\sigma''(\omega)] \tag{2}$$

where prime and double prime denote, respectively, the real and imaginary parts of $\varepsilon(\omega)$ and $\sigma(\omega)$. $\varepsilon(\omega)$ and $\sigma(\omega)$ are phenomenological coefficients that relate, respectively, the electric polarization and its time derivative (i.e., electric current) to the electric field. Therefore, $\varepsilon(\omega)$ and $\sigma(\omega)$ contain precisely the same information on the system's polarization dynamics. Because ionic systems are characterized by non-vanishing dc conductivity, i.e., $\sigma(0) = \sigma'(0) \neq 0$, we introduce $\varepsilon_c(\omega)$

$$\varepsilon_c(\omega) \equiv \varepsilon(\omega) - \mathrm{i}\frac{4\pi}{\omega}\sigma(0) = 1 + 4\pi\left[\chi(\omega) - \mathrm{i}\frac{\sigma(0)}{\omega}\right] \tag{3}$$

which does not diverge as ω approaches 0. Experimentally, the static dielectric constant ε_0 is determined as[3,4]

$$\varepsilon_0 = \varepsilon_c(0) = \lim_{\omega\to 0}\left[\varepsilon(\omega) - \mathrm{i}\frac{4\pi}{\omega}\sigma(0)\right] \tag{4}$$

The fluctuation−dissipation theorem relates $\chi(\omega)$ to the time correlation of $\mathbf{M}_{\mathrm{tot}}$ as

$$\chi(\omega) = -\frac{1}{3Vk_{\mathrm{B}}T}\int_0^\infty \mathrm{d}t\ \mathrm{e}^{\mathrm{i}\omega t}\frac{\mathrm{d}\Phi_{MM}(t)}{\mathrm{d}t}$$
$$\Phi_{MM}(t) = \langle \mathbf{M}_{\mathrm{tot}}(t)\cdot\mathbf{M}_{\mathrm{tot}}(0)\rangle \tag{5}$$

where k_{B} is Boltzmann's constant and T is the temperature. Following earlier works,[10,14] we decompose $\mathbf{M}_{\mathrm{tot}}$ into two components arising from reorientational and translational motions

$$\mathbf{M}_{\mathrm{tot}} = \mathbf{M}_{\mathrm{rot}}^{\mathrm{cm}} + \mathbf{M}_{\mathrm{tr}}^{\mathrm{cm}} \qquad \mathbf{M}_{\mathrm{rot}}^{\mathrm{cm}} \equiv \sum_\alpha \boldsymbol{\mu}_{\mathrm{cm},\alpha}$$
$$\mathbf{M}_{\mathrm{tr}}^{\mathrm{cm}} \equiv \sum_\alpha q_\alpha \mathbf{r}_{\mathrm{cm},\alpha}$$
$$\boldsymbol{\mu}_{\mathrm{cm},\alpha} = \sum_{i\in\alpha} q_{i,\alpha}(\mathbf{r}_{i,\alpha} - \mathbf{r}_{\mathrm{cm},\alpha}) \qquad q_\alpha = \sum_{i\in\alpha} q_{i,\alpha} \tag{6}$$

where q_α and $\mathbf{r}_{\mathrm{cm},\alpha}$ are the net charge and the position of the center of mass of ion α and $\boldsymbol{\mu}_{\mathrm{cm},\alpha}$ is its dipole moment with respect to its center of mass. $\chi(\omega)$ in eq 5 then becomes

$$\chi(\omega) = \chi_1^{\mathrm{cm}}(\omega) + \chi_2^{\mathrm{cm}}(\omega)$$
$$\chi_1^{\mathrm{cm}}(\omega) = \frac{1}{3Vk_{\mathrm{B}}T}\{\langle \mathbf{M}_{\mathrm{rot}}^{\mathrm{cm}2}\rangle + \int_0^\infty \mathrm{d}t\ \mathrm{e}^{\mathrm{i}\omega t}[\mathrm{i}\omega\Phi_{MM}^{\mathrm{cm}}(t) + \Phi_{MJ}^{\mathrm{cm}}(t)]\}$$
$$\chi_2^{\mathrm{cm}}(\omega) = \frac{1}{3Vk_{\mathrm{B}}T}\int_0^\infty \mathrm{d}t\ \mathrm{e}^{\mathrm{i}\omega t}\left[-\Phi_{JM}^{\mathrm{cm}}(t) + \frac{\mathrm{i}}{\omega}\Phi_{JJ}^{\mathrm{cm}}(t)\right]$$
$$\Phi_{MM}^{\mathrm{cm}}(t) = \langle \mathbf{M}_{\mathrm{rot}}^{\mathrm{cm}}(t)\cdot\mathbf{M}_{\mathrm{rot}}^{\mathrm{cm}}\rangle \qquad \Phi_{JJ}^{\mathrm{cm}}(t) = \langle \mathbf{J}_{\mathrm{tr}}^{\mathrm{cm}}(t)\cdot\mathbf{J}_{\mathrm{tr}}^{\mathrm{cm}}\rangle$$
$$\Phi_{MJ}^{\mathrm{cm}}(t) = \langle \mathbf{M}_{\mathrm{rot}}^{\mathrm{cm}}(t)\cdot\mathbf{J}_{\mathrm{tr}}^{\mathrm{cm}}\rangle \qquad \Phi_{JM}^{\mathrm{cm}}(t) = \langle \mathbf{J}_{\mathrm{tr}}^{\mathrm{cm}}(t)\cdot\mathbf{M}_{\mathrm{rot}}^{\mathrm{cm}}\rangle \tag{7}$$

where $\mathbf{J}_{\mathrm{tr}}^{\mathrm{cm}}$ is the ionic current due to the translational motions of ion center of mass

$$\mathbf{J}_{\mathrm{tr}}^{\mathrm{cm}} \equiv \frac{\mathrm{d}}{\mathrm{d}t}\mathbf{M}_{\mathrm{tr}}^{\mathrm{cm}} = \sum_\alpha q_\alpha \dot{\mathbf{r}}_{\mathrm{cm},\alpha} \tag{8}$$

and the cross-correlation functions satisfy $\Phi_{JM}^{\mathrm{cm}}(t) = -\Phi_{MJ}^{\mathrm{cm}}(t)$. It should be noted that, though ion reorientational motions about their center of mass are the main contributor to $\mathbf{M}_{\mathrm{rot}}^{\mathrm{cm}}$, their internal vibrations also make a contribution (see below). As in refs 14 and 15, we also introduce $\varepsilon_{\mathrm{rot}}^{\mathrm{cm}}(\omega)$ and $\varepsilon_{\mathrm{tr}}^{\mathrm{cm}}(\omega)$

$$\varepsilon_{\mathrm{rot}}^{\mathrm{cm}}(\omega) \equiv 1 + 4\pi\chi_1^{\mathrm{cm}}(\omega)$$
$$\varepsilon_{\mathrm{tr}}^{\mathrm{cm}}(\omega) \equiv \varepsilon_c(\omega) - \varepsilon_{\mathrm{rot}}^{\mathrm{cm}}(\omega) = 4\pi\left[\chi_2^{\mathrm{cm}}(\omega) - \mathrm{i}\frac{\sigma(0)}{\omega}\right] \tag{9}$$

The decomposition of $\mathbf{M}_{\mathrm{tot}}$ via eq 6 and thus of $\varepsilon_c(\omega)$ into $\varepsilon_{\mathrm{rot}}^{\mathrm{cm}}(\omega)$ and $\varepsilon_{\mathrm{tr}}^{\mathrm{cm}}(\omega)$ via eqs 7−9 has an important advantage in that it enables us to understand characteristics of different molecular motions in ILs and their roles in the dielectric relaxation and related phenomena. Reorientational (plus vibrational) and translational motions of ions and their cross-correlations contribute to $\chi_1^{\mathrm{cm}}(\omega)$ and $\chi_2^{\mathrm{cm}}(\omega)$ of ILs (eq 7). Because translational and reorientational motions are usually decoupled, the contribution of the cross-terms is very small. Therefore, $\varepsilon_{\mathrm{rot}}^{\mathrm{cm}}(\omega)$ and $\varepsilon_{\mathrm{tr}}^{\mathrm{cm}}(\omega)$ arise primarily from reorientations (and vibrations) of individual ions with respect to, and translations of, their center of mass and thus can shed light on details of ion dynamics in ILs. We nonetheless note that the decomposition is for convenience and that physically measurable quantities such as $\chi(\omega)$ and $\varepsilon(\omega)$ do not and should not depend on the decomposition scheme employed.

Simulation Models and Methods. Molecular dynamics simulations were performed in the isothermal−isobaric (NPT) ensemble using the GROMACS simulation package.[41] Nosé−Hoover temperature coupling and Parrinello−Rahman pressure coupling were used. A fully flexible but nonpolarizable all-atom description based on the OPLS-AA force fields[42] was employed to describe intermolecular interactions. Specifically, the force field parameters of ref 43 were used for 1-ethyl-3-methylimidazolium (EMI^+), whereas the parameters for ethyl sulfate (ETS^-) were taken from ref 44. The simulation cell comprises 128 pairs of EMI^+ and ETS^- ions in a cubic box with periodic conditions applied. The long-range electrostatic interactions were computed via the particle-mesh-Ewald

DOI: 10.1021/acs.jpcb.7b00160
J. Phys. Chem. B 2017, 121, 4845−4852

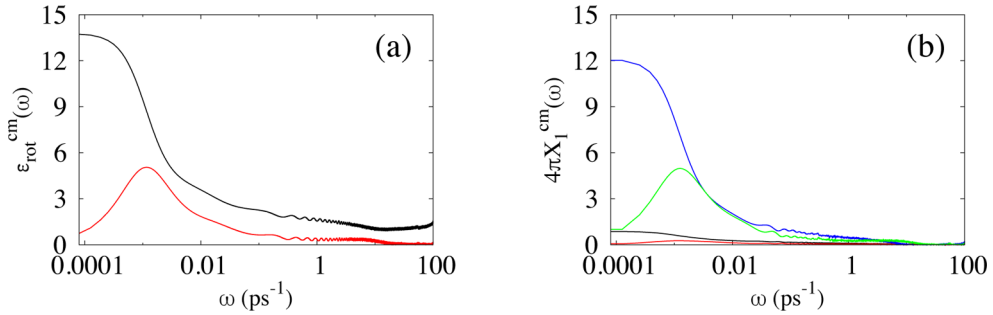

Figure 1. MD results for (a) the real (black) and imaginary (red) parts of $\varepsilon_{rot}^{cm}(\omega)$ and (b) the respective contributions of the anion and cation center-of-mass dipole moments. In (b), the anion contributions are displayed in blue (real) and green (imaginary) and the cation contributions in black (real) and red (imaginary), respectively. The contribution from the cross-correlation of the anion and cation center-of-mass dipoles is small and thus is not shown.

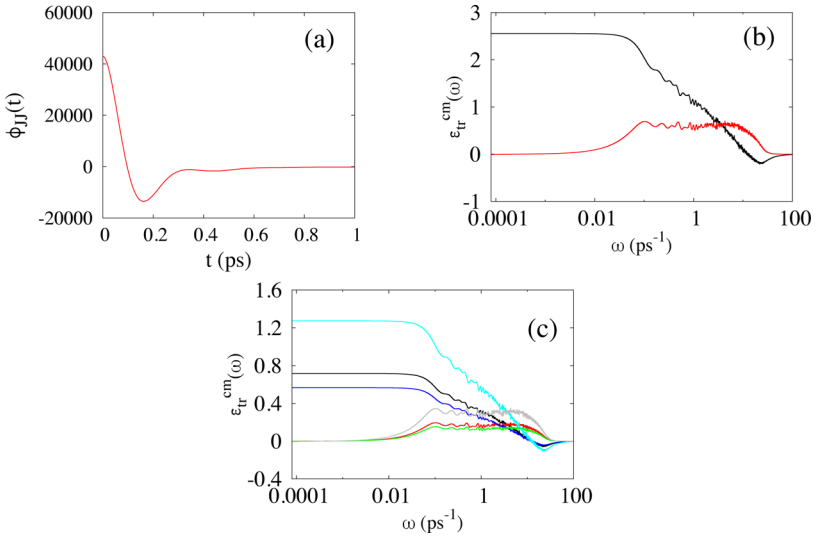

Figure 2. MD results for (a) $\Phi_{JJ}^{cm}(t)$, (b) $\varepsilon_{tr}^{cm}(\omega)$, and (c) contributions to $\varepsilon_{tr}^{cm}(\omega)$ from the autocorrelations of the anion and cation currents and their cross-correlations. In (b), the real and imaginary parts of $\varepsilon_{tr}^{cm}(\omega)$ are displayed in black and red, respectively. In (c) the anion contributions are plotted in blue (real) and green (imaginary) and the cation contributions in black (real) and red (imaginary), and the contributions of their cross-terms are presented in cyan (real) and gray (imaginary). The total $\varepsilon_{tr}^{cm}(\omega)$ in (b) is the sum of the anion, cation and cross-terms in (c).

method, resulting in essentially no truncation of these interactions. Three trajectories were simulated at 350 K and 1 atm, using the Verlet leapfrog algorithm with a time step of 1 fs. For each trajectory, simulation was carried out with 1.5 ns of annealing from 600 K and 10 ns of equilibration at 350 K, followed by a 30 ns production run. Averages were computed using three 30 ns trajectories thus generated, corresponding to a total of 90 ns simulation.

RESULTS AND DISCUSSION

Dielectric Relaxation. At the outset, we mention that cross-correlations, $\Phi_{JM}^{cm}(t)$ and $\Phi_{MJ}^{cm}(t)$, between the collective center-of-mass dipole moment $\mathbf{M}_{rot}^{cm}(t)$ and the ionic current $\mathbf{J}_{tr}^{cm}(t)$ are found to be insignificant and thus do not play any important role in $\varepsilon_{rot}^{cm}(\omega)$ or $\varepsilon_{tr}^{cm}(\omega)$ for the EMI^+ETS^- system studied here. With this in mind, we first consider $\varepsilon_{rot}^{cm}(\omega)$ in Figure 1, which arises from ion reorientational dynamics. Most noticeable is a strong band at $\omega \approx 1.2 \times 10^{-3}$ ps^{-1} ($f \approx 0.2$ GHz), which spans a very broad frequency range from $\omega \approx 0.001$ to 0.1 ps^{-1}. The monotonically decreasing behavior of $\varepsilon_{rot}^{cm\prime}(\omega)$ with the increasing frequency clearly indicates that this band is due to dissipative modes. For additional insight, we analyzed the respective contributions of the cations and anions. The results in Figure 1b show that the gigahertz band is dominated by the anions. This is as expected because the center-of-mass dipole moment 7.19 D for ETS^- is much larger than 1.94 D for EMI^+ in the force-field description[43,44] employed in our study. All other things being equal, the peak intensity will be proportional to square dipole moment because $\mathbf{M}_{rot}^{cm}$ scales linearly with the center-of-mass dipole moment (eqs 6 and 7). We also notice that the anion peak is shifted toward higher frequencies, compared to the cation peak. This suggests that the anion reorientations are slightly faster than the cation reorientations (results not shown).

Recently, the microwave region of EMI^+ETS^- was studied via dielectric relaxation spectroscopy.[40] Though in good qualitative agreement, we note a couple of differences. First, the MD prediction for the peak frequency of the gigahertz band is lower than the experimental result ($\omega \approx 7 \times 10^{-3}$ ps^{-1})[40] by a factor of ~6. This is not surprising in that nonpolarizable force-field models for ILs with integral ionic charges tend to underestimate their transport coefficients considerably. This state of affairs would be improved with the inclusion of electronic polarizability in the potential model; according to previous studies,[45−48] it would accelerate IL transport dynamics by a factor of $\lesssim$2. Another difference is the assignment of the

DOI: 10.1021/acs.jpcb.7b00160
J. Phys. Chem. B 2017, 121, 4845−4852

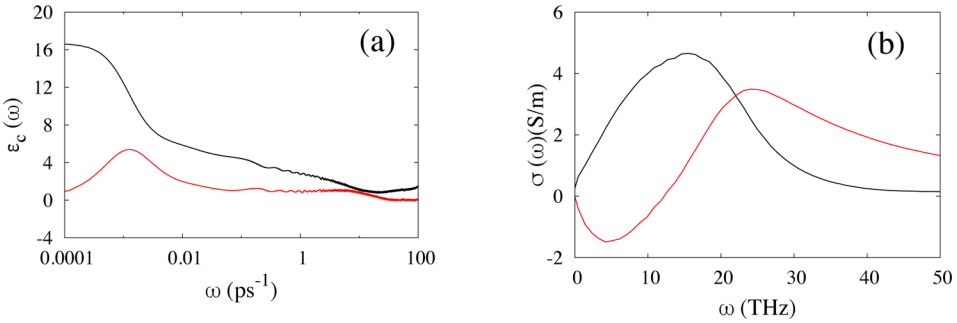

Figure 3. Frequency-dependent (a) dielectric constant $\varepsilon_c(\omega)$ in eq 3 and (b) ionic conductivity $\sigma(\omega)$ in eq 2. The real and imaginary parts are plotted in black and red, respectively.

gigahertz band; although we attribute it primarily to anions as discussed above, it is assigned mainly to cation reorientations in ref 40.

Another interesting aspect of Figure 1b is that though weak in intensity, the anions yield a discernible band structure in the frequency range between ∼1 and ∼20 ps^{-1}. The result that $\varepsilon_{\mathrm{rot}}^{\mathrm{cm}\prime}(\omega)$ shows a transition from the anomalous to normal dispersion near ω = 10 ps^{-1} indicates that this absorption mode has a resonance character. This is ascribed to hindered rotations of ETS$^-$. We note that the terahertz structure of $\varepsilon_{\mathrm{rot}}^{\mathrm{cm}}(\omega)$ arising from anion vibrations observed here was absent in EMI$^+$PF$_6^-$ studied in ref 14 because of the highly symmetric structure of PF$_6^-$.

The value of $4\pi\chi_1^{\mathrm{cm}}(0)$ $(=\varepsilon_{\mathrm{rot}}^{\mathrm{cm}\prime}(0) - 1)$, 12.8, measures the contribution of mainly ion reorientations to the static dielectric constant ε_0 of the IL system (Figure 1a). The contribution of the anions (12.0) is much higher than that of the cations (0.8) (Figure 1b) for precisely the same reason the $\varepsilon_{\mathrm{rot}}^{\mathrm{cm}\prime\prime}(\omega)$ peak in the gigahertz region above is much more intense for the former than the latter. The cationic contribution to $\varepsilon_{\mathrm{rot}}^{\mathrm{cm}\prime}(0)$ obtained here compares very well with that for the EMI$^+$PF$_6^-$ system studied in ref 14. However, the overall $\varepsilon_{\mathrm{rot}}^{\mathrm{cm}\prime}(0)$ value of the EMI$^+$ETS$^-$ system is much higher than that of EMI$^+$PF$_6^-$ as PF$_6^-$ anions of the latter IL do not contribute to $\varepsilon_{\mathrm{rot}}^{\mathrm{cm}\prime}(0)$ due to their high spherical symmetry.

We turn to $\Phi_{JJ}^{\mathrm{cm}}(t)$ and $\varepsilon_{\mathrm{tr}}^{\mathrm{cm}}(\omega)$ in Figure 2. As mentioned above, the cross-correlation between $\mathbf{M}_{\mathrm{rot}}^{\mathrm{cm}}(t)$ and $\mathbf{J}_{\mathrm{tr}}^{\mathrm{cm}}(t)$ is negligible, so that $\varepsilon_{\mathrm{tr}}^{\mathrm{cm}}(\omega)$ is governed essentially by the current autocorrelation $\Phi_{JJ}^{\mathrm{cm}}(t)$ (cf. eq 7), i.e., ion translational dynamics. The dc conductivity needed in the calculation of $\varepsilon_{\mathrm{tr}}^{\mathrm{cm}}(\omega)$ (eq 9) was determined via

$$\sigma(0) = -\mathrm{i}\lim_{\omega\to 0}\omega\chi(\omega) = \frac{1}{3Vk_{\mathrm{B}}T}\int_0^\infty \mathrm{d}t\ \Phi_{JJ}^{\mathrm{cm}}(t) \tag{10}$$

Analogous to other imidazolium-based ILs,[11,14,15,49] $\Phi_{JJ}^{\mathrm{cm}}(t)$ in Figure 2a exhibits a rapid oscillatory decay, followed by dissipative relaxation. Its oscillation period is found to be ∼0.3 ps, and the ionic current becomes strongly anticorrelated, viz., $\Phi_{JJ}^{\mathrm{cm}}(t) < 0$, in less than 0.2 ps. This reveals the librational character of ion translational motions at short times. The relaxation of $\Phi_{JJ}^{\mathrm{cm}}(t)$ is nearly completed in less than 1 ps, indicating that its main contribution to $\varepsilon_c(\omega)$ occurs in the terahertz frequency region. As shown in Figure 2b, $\varepsilon_{\mathrm{tr}}^{\mathrm{cm}}(\omega)$ is characterized by a significant absorption band in the 0.1 ps^{-1} $\lesssim \omega \lesssim$ 20 ps^{-1} (0.015 THz $\lesssim f \lesssim$ 3 THz) region. The transition from the anomalous to normal dispersion in $\varepsilon_{\mathrm{tr}}^{\mathrm{cm}\prime}(\omega)$ near ω = 20 ps^{-1} confirms that the absorption mode there has a resonance character (i.e., oscillatory decay of $\Phi_{JJ}^{\mathrm{cm}}(t)$),[14,15] which was indeed observed in a recent spectroscopic study.[50] The broad and multipeak character of the terahertz band suggests that there is at least one more mode near ω = 0.3 ps^{-1}. This sub-terahertz mode is ascribed to dissipative relaxation of $\Phi_{JJ}^{\mathrm{cm}}(t)$ mentioned above.[13,15] $\sigma(0)$ calculated via the Green−Kubo formula, eq 10, is 0.26 S/m, whereas the Einstein−Helfand relation[13,15] yields 0.24 S/m. The sub-terahertz mode shows a considerable overlap with the high-frequency end of $\varepsilon_{\mathrm{rot}}^{\mathrm{cm}\prime}(\omega)$ in Figure 1a.

It should be noted that $\varepsilon_{\mathrm{tr}}^{\mathrm{cm}}(\omega)$ does not vanish at ω = 0. Though it may not be large in magnitude, $\varepsilon_{\mathrm{tr}}^{\mathrm{cm}}(0)$ of ∼2.5 nonetheless corresponds to about 20% of the zero-frequency value of $\varepsilon_{\mathrm{rot}}^{\mathrm{cm}}(\omega) - 1$, arising from ion reorientational dynamics. This clearly indicates that ion translations make a nonnegligible contribution to the static dielectric constant of IL.[14,15] From eqs 7 and 9, one can obtain

$$\begin{aligned}\varepsilon_{\mathrm{tr}}^{\mathrm{cm}}(0) &= 4\pi\chi_2^{\mathrm{cm}}(0)\\ &= -\frac{4\pi}{3Vk_{\mathrm{B}}T}\lim_{\omega\to 0}\int_0^\infty \mathrm{d}t\ \frac{\sin\omega t}{\omega}\Phi_{JJ}^{\mathrm{cm}}(t)\\ &= -\frac{4\pi}{3Vk_{\mathrm{B}}T}\int_0^\infty \mathrm{d}t\ t\Phi_{JJ}^{\mathrm{cm}}(t)\end{aligned} \tag{11}$$

The last expression of eq 11 reveals that the positive $\varepsilon_{\mathrm{tr}}^{\mathrm{cm}}(0)$ value is due to the aforementioned strong anticorrelation of $\Phi_{JJ}^{\mathrm{cm}}(t)$; i.e., the current autocorrelation function becomes negative-valued during relaxation.[14] According to ref 15, $\varepsilon_{\mathrm{tr}}^{\mathrm{cm}}(0)$ and $\varepsilon_{\mathrm{rot}}^{\mathrm{cm}}(0)$, respectively, increase and decrease with temperature. This antagonistic behaviors of $\varepsilon_{\mathrm{tr}}^{\mathrm{cm}}(0)$ and $\varepsilon_{\mathrm{rot}}^{\mathrm{cm}}(0)$ result in a weak overall T-dependence of the IL dielectric constant.

For additional insight, respective contributions of the cations and anions and their cross-terms to $\varepsilon_{\mathrm{tr}}^{\mathrm{cm}}(\omega)$ are compared in Figure 2c. The most noteworthy feature is that the contribution of the cation−anion cross-correlation is comparable to the contributions of the cation and anion autocorrelations. Furthermore, the two autocorrelations and the cross-correlation yield exactly the same terahertz band structures. Because of the conservation of momentum, collective translational motions of the cations and the anions are fully correlated, i.e.,

$$\begin{aligned}\sum_{\alpha\in\text{cations}} m^{(+)}\dot{\mathbf{r}}_{\mathrm{cm},\alpha} + \sum_{\alpha\in\text{anions}} m^{(-)}\dot{\mathbf{r}}_{\mathrm{cm},\alpha} &= 0\\ m^{(+)}\mathbf{J}_{\mathrm{tr}}^{(+)} &= m^{(-)}\mathbf{J}_{\mathrm{tr}}^{(-)}\end{aligned} \tag{12}$$

where $m^{(\pm)}$ and $\mathbf{J}_{\mathrm{tr}}^{(\pm)}$ are the masses and ionic currents of the cations and anions. Therefore, the temporal behaviors of the autocorrelations of $\mathbf{J}_{\mathrm{tr}}^{(+)}$ and $\mathbf{J}_{\mathrm{tr}}^{(-)}$ and their cross-correlation are identical. Because $m^{(+)}$ = 112 amu and $m^{(-)}$ = 125 amu, $\mathbf{J}_{\mathrm{tr}}^{(-)}$ =

DOI: 10.1021/acs.jpcb.7b00160
J. Phys. Chem. B 2017, 121, 4845−4852

$0.9\mathbf{J}_{tr}^{(+)}$. As a result, the ratio of the contributions to $\varepsilon_{tr}^{cm}(\omega)$ from the $\mathbf{J}_{tr}^{(+)}$ autocorrelation, the $\mathbf{J}_{tr}^{(-)}$ autocorrelation, and their two cross-correlation terms are 1:0.81:1.8.

For completeness, the full dielectric response function $\varepsilon_c(\omega)$ $(=\varepsilon_{rot}^{cm}(\omega) + \varepsilon_{tr}^{cm}(\omega))$ and the conductivity $\sigma(\omega)$ (eq 2) are presented in Figure 3. The absorption intensity indicates that the main dielectric loss in EMI^+ETS^- occurs in the microwave region via ion reorientations. Nevertheless, ion translational and rovibrational dynamics yield a broad band consisting of multiple resonance and dissipative modes in the far-IR region as analyzed above.

The MD result for the overall dielectric constant for EMI^+ETS^- is 16.2 at 350 K. Because no dielectric measurements have been made at this temperature to our knowledge, we have estimated the experimental value of ε_0 by extrapolating the results reported in ref 40. Regardless of the fitting functions we used, we obtained $\varepsilon_0 \approx 24-26$ at 350 K. The disagreement between the MD and experimental estimate indicates the limitations of the force-field model description, such as the absence of electronic polarizability, employed in the present work. For example, an increase in the ion center-of-mass dipole by ~20% would increase the contribution of ion reorientations to ε_0 by ~45% from 12 to ~17.5 for anions and from 1.8 to ~2.6 for cations. All other things being equal, this would result in the overall dielectric constant of ~22.5. The incorporation of the acidic nature of the ring hydrogen atom at the C2 position of EMI^+ into the force field parametrization would also increase the cation contribution to ε_0. Another potential source for the disagreement is the uncertainties in the experimental determination of ε_0; for instance, at 298 K, the ε_0 value reported in ref 40 is 35.2 whereas it is 27.9 in ref 21.

We also note that unlike the dipolar solvents, the interaction-induced contributions to FIR of EMI^+ETS^- are reasonably captured in MD despite the neglect of electronic polarizability. To understand this point better, we consider as an example the well-known 180 cm^{-1} mode present in the FIR (and depolarized Raman) spectrum of water, arising from intermolecular hydrogen bond stretching motions. If the electronic polarizability of water is ignored, the total dipole moment $\mathbf{M}_{tot}$ of the system is no longer modulated by relative translational motions of water because dipole moments of electrically neutral molecules are invariant under translations. This means that intermolecular hydrogen bond stretching motions do not influence $\mathbf{M}_{tot}$ and, as a result, the 180 cm^{-1} band will disappear in FIR of water determined with nonpolarizable force fields.[51] By contrast, relative translational motions of nonpolarizable ions do alter the total dipole moment of the IL system because they all have nonvanishing charges. Therefore, fluctuations of intermolecular interactions via ion translations are reflected to a large extent in the MD result for FIR of EMI^+ETS^-. The presence of the terahertz band in $\varepsilon_{tr}^{cm}(\omega)$ discussed above is a direct consequence of this feature.

Comparison with Experimental Data. Finally, we compare the MD predictions with experimental results for the low-frequency spectrum of EMI^+ETS^-. To this end, an OKE experiment was carried out at T = 298 K. Details of the experimental setup and procedure can be found elsewhere.[17,52,53] To avoid any confusion, we should note that OKE is a time-domain analog of conventional depolarized Raman spectroscopy, whereas FIR is an absorption technique. Hence, their selection rules are different (i.e., polarizability anisotropy vs dipole fluctuations) and some modes will appear only in one of the two spectra.

With this difference in mind, we proceed to the low-frequency OKE spectrum of EMI^+ETS^- and its fitted profiles in Figure 4. The individual profiles represent different contributions to the OKE signal. At the very low frequency end, the signal is dominated by rotational diffusion, which is modeled as a Cole–Davidson function with an inertial rise. The very broad feature peaking around 0.02 THz is modeled as a logarithmic decay with an inertial rise and termination at the low-frequency end. The dominant librational mode is the broad band peaking at about 2.5 THz. It is represented by a convolution of Gaussian and Brownian oscillators to account for inhomogeneous and homogeneous broadening, respectively. The peaks at higher frequencies are well reproduced by homogeneously broadened profiles. For details on the data analysis and theoretical considerations, the reader is referred to ref 17.

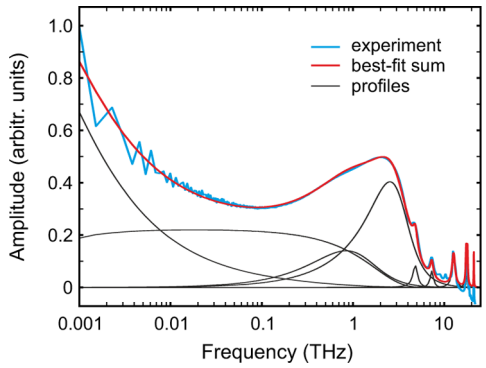

Figure 4. Experimental OKE spectrum and fitted profiles.

In Figure 5a, the experimental OKE spectrum ($\lesssim$700 cm^{-1}) and the simulated IR spectrum calculated by Fourier transformation of the total dipole moment correlation are compared. Although some peaks in the experimental OKE spectrum agree well with the MD results for FIR, some other OKE peaks are not reflected in the computational spetrum. One of the possible reasons for this discrepancy is the difference in temperature, i.e., 298 K for OKE vs 350 K for FIR. However, according to previous simulation studies of imidazolium-based ILs,[15,54] frequencies of resonance modes in dielectric loss and time-resolved fluorescence spectroscopies are not that sensitive to temperature though their intensities, especially in the former, are. Another reason is the difference in selection rules as mentioned above. For example, the broad band in the range 10–150 cm^{-1} with a peak at 67 cm^{-1} in the experimental OKE spectrum shows a rather significant deviation from the calculated FIR structure at 118 cm^{-1}. However, a closer look at Figure 5b, in which the rovibrational and translational contributions of the ions to the computational spectrum are displayed, suggests that the broad OKE band at 67 cm^{-1} is governed mainly by the rovibrational motions, in particular, hindered rotations, of anions. In this sense, a shoulder structure around 130 cm^{-1} in the anion rovibrational component in the MD results correlates reasonably well with the OKE peak at 155 cm^{-1}. Nonetheless other motions, such as hindered translations of ions responsible for the FIR peak at 118 cm^{-1}, can also contribute.

In the range between 200 and 500 cm^{-1}, the experimental OKE spectrum exhibits peaks at 243, 297, 345, and 422 cm^{-1}. In the computed IR spectrum, a couple of weak translational

DOI: 10.1021/acs.jpcb.7b00160
J. Phys. Chem. B 2017, 121, 4845–4852

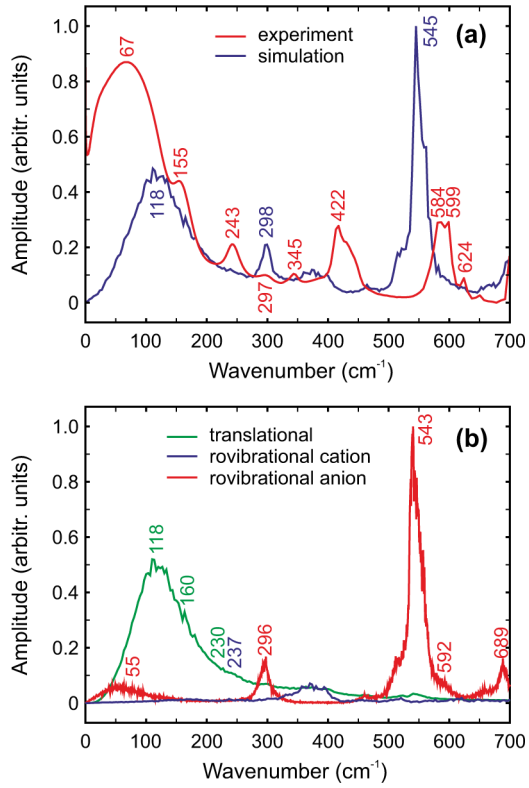

Figure 5. Comparison of the computational IR spectrum with OKE experiment. (a) Experimental OKE and computational IR spectrum. (b) Translational and rovibrational contributions extracted from the MD data.

and cationic rovibrational modes can be found around 240 cm^{-1}; its very weak structure at 237 cm^{-1} is mainly due to the cation methyl group (analysis not shown). The computational band centered at 298 cm^{-1}, arising primarily from the ethyl group of the anion (cf. Figure 5b), shows an excellent agreement with the peak at 297 cm^{-1} in the OKE spectrum. The experimental peaks at 345 and 422 cm^{-1} are in very good accord with previous Raman data[29] with peaks at 339 and 413 cm^{-1}, assigned to O−S−O bending vibrations of the anion. The MD results, however, exhibit a weak but broad band in this range, which is attributed mainly to the ethyl group of the cation. It should nonetheless be noted that the experimental data exhibit a low-intensity shoulder around 390 cm^{-1}, in agreement with the simulated spectrum. At higher wavenumbers, the OKE spectrum shows a pronounced double-peak structure around 590 cm^{-1}, whereas the simulated spectrum exhibits a very strong peak at 545 cm^{-1} with a shoulder structure at both wings. The comparison with previous Raman and IR analysis[29] indicates that these spectral features have different origins. The OKE peaks agree well with the Raman mode at 596 cm^{-1}, assigned to an N−C stretching vibration of the cation, whereas the peak in the simulated IR spectrum arises from rovibrational modes, in particular, SO_3 wag, of the anion.

The absorption spectra of EMI^+ETS^- in the terahertz region have been studied by Wulf et al.[55] They found pronounced peaks at 106 and 245 cm^{-1} with minor structures around 160 and 295 cm^{-1}. The latter three are in good accord with the experimental OKE and the MD results. In addition, the absorption peak at 106 cm^{-1} shows a reasonable agreement with the broad band at 118 cm^{-1} in the simulated IR spectrum, arising from hindered translations. Interestingly, when the very broad low-frequency region of the OKE spectrum was analyzed through fitting as described above (i.e., a logarithmic decay with an inertial rise and low-frequency termination), it yielded a peak at 98.4 cm^{-1} (Figure 4). This is in reasonable agreement with the absorption peak at 118 cm^{-1}. Wulf et al. assigned this peak to the stretching vibration of the interionic hydrogen bond.

CONCLUSION

In this article, we reported a detailed analysis of the far-IR, dielectric relaxation, and conductivity behaviors of EMI^+ETS^- by employing MD simulations. The analysis of ion reorientational dynamics predicts that ETS^- anions play a major role in dielectric relaxation in the gigahertz and lower frequency regions because their center-of-mass dipole moment is much larger than that of EMI^+ cations. By contrast, both cations and anions and their cross-correlations make significant contributions to dielectric relaxation in the terahertz domain through hindered translational motions. Our analysis indicated that low-frequency vibrations of anions, in particular, bending motions involving their CH_3 and CH_2 groups also contribute to the terahertz region though their contributions are much smaller than those of ion translational dynamics.

Comparison of the simulated far-IR spectrum and experimental OKE spectrum yielded good agreement between the two, especially in the low-frequency region. This indicates that, despite the approximate nature of the force-field model employed in our study, it captures key reorientational, translational, and low-frequency vibrational motions of ions correctly and nearly at the quantitative level. In this respect, our analysis here contributes important insight into understanding of individual and collective ion dynamics in EMI^+ETS^-.

AUTHOR INFORMATION

Corresponding Author

*H. J. Kim. E-mail: hjkim@cmu.edu.

ORCID

Johannes Kiefer: 0000-0002-0837-3456
Klaas Wynne: 0000-0002-5305-5940
Hyung J. Kim: 0000-0003-4334-1879

Present Address

⊥Carnegie Mellon University.

Notes

The authors declare no competing financial interest.

ACKNOWLEDGMENTS

This work was supported in part by the National Science Foundation through NSF Grant No. CHE-1223988 and by EPSRC Grants Nos. EP/K00090X/1, EP/J009733/1, and EP/K034995/1.

REFERENCES

(1) Goulon, J.; Rivail, J. L. Dielectric relaxation and far infrared dispersion in pure liquid chloroform. *Chem. Phys. Lett.* **1973**, *18*, 211−216.

(2) Fulton, R. L. Dipole correlations in conducting media. *J. Chem. Phys.* **1978**, *68*, 3095−3098.

(3) Hubbard, J. B.; Colonomos, P.; Wolynes, P. G. Molecular theory of solvated ion dynamics. III. The kinetic dielectric decrement. *J. Chem. Phys.* **1979**, *71*, 2652−2661.

DOI: 10.1021/acs.jpcb.7b00160
J. Phys. Chem. B 2017, 121, 4845−4852

(4) Caillol, J. M.; Levesque, D.; Weis, J. J. Theoretical calculation of ionic solution properties. *J. Chem. Phys.* **1986**, *85*, 6645−6657.
(5) Caillol, J. M.; Levesque, D.; Weis, J. J. Electrical properties of polarizable ionic solutions. I. Theoretical aspects. *J. Chem. Phys.* **1989**, *91*, 5544−5554.
(6) Kim, H. J.; Friedman, H. L.; Raineri, F. O. Smoluchowski fluctuation theory of dielectric relaxation. *J. Chem. Phys.* **1991**, *94*, 1442−1453.
(7) Wei, D.; Patey, G. N. Dielectric relaxation of electrolyte solutions. *J. Chem. Phys.* **1991**, *94*, 6795−6806.
(8) Chandra, A.; Wei, D.; Patey, G. N. Dielectric relaxation of electrolyte solutions: Is there really a kinetic dielectric decrement? *J. Chem. Phys.* **1993**, *98*, 4959−4966.
(9) Chandra, A. Static dielectric constant of aqueous electrolyte solutions: Is there any dynamic contribution? *J. Chem. Phys.* **2000**, *113*, 903−905.
(10) Schröder, C.; Wakai, C.; Weingärtner, H.; Steinhauser, O. Collective rotational dynamics in ionic liquids: A computational and experimental study of 1-butyl-3-methyl-imidazolium tetrafluoroborate. *J. Chem. Phys.* **2007**, *126*, 084511−13.
(11) Schröder, C.; Haberler, M.; Steinhauser, O. On the computation and contribution of conductivity in molecular ionic liquids. *J. Chem. Phys.* **2008**, *128*, 134501−10.
(12) Schröder, C.; Steinhauser, O. On the dielectric conductivity of molecular ionic liquids. *J. Chem. Phys.* **2009**, *131*, 114504.
(13) Schröder, C. Collective translational motions and cage relaxations in molecular ionic liquids. *J. Chem. Phys.* **2011**, *135*, 024502−11.
(14) Shim, Y.; Kim, H. J. Dielectric Relaxation, Ion Conductivity, Solvent Rotation, and Solvation Dynamics in a Room-Temperature Ionic Liquid. *J. Phys. Chem. B* **2008**, *112*, 11028−11038.
(15) Shim, Y.; Kim, H. J. Dielectric Relaxation and Solvation Dynamics in a Room-Temperature Ionic Liquid: Temperature Dependence. *J. Phys. Chem. B* **2013**, *117*, 11743−11752.
(16) Stoppa, A.; Hunger, J.; Buchner, R.; Hefter, G.; Thoman, A.; Helm, H. Interactions and Dynamics in Ionic Liquids. *J. Phys. Chem. B* **2008**, *112*, 4854−4858.
(17) Turton, D. A.; Hunger, J.; Stoppa, A.; Hefter, G.; Thoman, A.; Walther, M.; Buchner, R.; Wynne, K. Dynamics of Imidazolium Ionic Liquids from a Combined Dielectric Relaxation and Optical Kerr Effect Study: Evidence for Mesoscopic Aggregation. *J. Am. Chem. Soc.* **2009**, *131*, 11140−11146.
(18) Turton, D. A.; Sonnleitner, T.; Ortner, A.; Walther, M.; Hefter, G.; Seddon, K. R.; Stana, S.; Plechkova, N. V.; Buchner, R.; Wynne, K. Structure and dynamics in protic ionic liquids: A combined optical Kerr-effect and dielectric relaxation spectroscopy study. *Faraday Discuss.* **2012**, *154*, 145−153.
(19) Weingärtner, H.; Sasisanker, P.; Daguenet, C.; Dyson, P. J.; Krossing, I.; Slattery, J. M.; Schubert, T. The Dielectric Response of Room-Temperature Ionic Liquids:A Effect of Cation Variation. *J. Phys. Chem. B* **2007**, *111*, 4775−4780.
(20) Wakai, C.; Oleinikova, A.; Ott, M.; Weingärtner, H. How Polar Are Ionic Liquids? Determination of the Static Dielectric Constant of an Imidazolium-based Ionic Liquid by Microwave Dielectric Spectroscopy. *J. Phys. Chem. B* **2005**, *109*, 17028−17030.
(21) Weingärtner, H. Z. The Static Dielectric Constant of Ionic Liquids. *Z. Phys. Chem.* **2006**, *220*, 1395−1405.
(22) Schröder, C.; Hunger, J.; Stoppa, A.; Buchner, R.; Steinhauser, O. On the collective network of ionic liquid/water mixtures. II. Decomposition and interpretation of dielectric spectra. *J. Chem. Phys.* **2008**, *129*, 184501−10.
(23) Izgorodina, E. I.; Forsyth, M.; MacFarlane, D. R. On the components of the dielectric constants of ionic liquids: ionic polarization? *Phys. Chem. Chem. Phys.* **2009**, *11*, 2452−2458.
(24) For an extensive list of experimental and theoretical works on solvatochromism in ILs, see ref 15.
(25) Holbrey, J. D.; Reichert, W. M.; Swatloski, R. P.; Broker, G. A.; Pitner, W. R.; Seddon, K. R.; Rogers, R. D. Efficient, halide free synthesis of new, low cost ionic liquids: 1,3-dialkylimidazolium salts containing methyl- and ethyl-sulfate anions. *Green Chem.* **2002**, *4*, 407−413.
(26) Böwing, A. G.; Jess, A. Kinetics and reactor design aspects of the synthesis of ionic liquids-Experimental and theoretical studies for ethylmethylimidazole ethylsulfate. *Chem. Eng. Sci.* **2007**, *62*, 1760−1769.
(27) Pereiro, A. B.; Deive, F. J.; Esperanca, J. M. S. S.; Rodriguez, A. Alkylsulfate-based ionic liquids to separate azeotropic mixtures. *Fluid Phase Equilib.* **2010**, *294*, 49−53.
(28) Kiefer, J.; Fries, J.; Leipertz, A. Experimental Vibrational Study of Imidazolium-Based Ionic Liquids: Raman and Infrared Spectra of 1-Ethyl-3-methylimidazolium Bis(trifluoromethylsulfonyl)imide and 1-Ethyl-3-methylimidazolium Ethylsulfate. *Appl. Spectrosc.* **2007**, *61*, 1306−1311.
(29) Dhumal, N. R.; Kim, H. J.; Kiefer, J. Electronic Structure and Normal Vibrations of the 1-Ethyl-3-methylimidazolium Ethyl Sulfate Ion Pair. *J. Phys. Chem. A* **2011**, *115*, 3551−3558.
(30) Kozlov, D. N.; Kiefer, J.; Seeger, T.; Fröba, A. P.; Leipertz, A. Determination of Physicochemical Parameters of Ionic Liquids and Their Mixtures with Solvents Using Laser-Induced Gratings. *J. Phys. Chem. B* **2011**, *115*, 8528−8533.
(31) Fumino, K.; Reimann, S.; Ludwig, R. Probing molecular interaction in ionic liquids by low frequency spectroscopy: Coulomb energy, hydrogen bonding and dispersion forces. *Phys. Chem. Chem. Phys.* **2014**, *16*, 21903−21929.
(32) Kiefer, J.; Namboodiri, M.; Kazemi, M.; Materny, A. Time-resolved femtosecond CARS of the ionic liquid 1-ethyl-3-methyl-imidazolium ethylsulfate. *J. Raman Spectrosc.* **2015**, *46*, 722−726.
(33) Vila, J.; Varela, L. M.; Cabeza, O. Cation and anion sizes influence in the temperature dependence of the electrical conductivity in nine imidazolium based ionic liquids. *Electrochim. Acta* **2007**, *52*, 7413−7417.
(34) Calado, M. S.; Diogo, C.; Correia da Mata, J. L.; Caetano, J. P.; Visak, Z. P.; Fareleira, M. N. A. Electrolytic Conductivity of Four Imidazolium-Based Ionic Liquids. *Int. J. Thermophys.* **2013**, *34*, 1265−1279.
(35) Gardas, R.; Coutinho, A. P. A Group Contribution Method for Heat Capacity Estimation of Ionic Liquids. *Ind. Eng. Chem. Res.* **2008**, *47*, 5751−5757.
(36) Bica, K.; Deetlefs, M.; Schröder, C.; Seddon, K. R. Polarisabilities of alkylimidazolium ionic liquids. *Phys. Chem. Chem. Phys.* **2013**, *15*, 2703−2711.
(37) Malberg, F.; Brehm, M.; Holloczki, O.; Pensado, A. S.; Kirchner, B. Understanding the evaporation of ionic liquids using the example of 1-ethyl-3-methylimidazolium ethylsulfate. *Phys. Chem. Chem. Phys.* **2013**, *15*, 18424−18436.
(38) Santos, C. S.; Baldelli, S. Alkyl Chain Interaction at the Surface of Room Temperature Ionic Liquids: Systematic Variation of Alkyl Chain Length (R = C1-C4, C8) in both Cation and Anion of [RMIM][R-OSO3] by Sum Frequency Generation and Surface Tension. *J. Phys. Chem. B* **2009**, *113*, 923−933.
(39) Gottfried, J. M.; Maier, F.; Rossa, J.; Gerhand, D.; Schulz, P. S.; Wasserscheid, P.; Steinrück, H. P. Surface Studies on the Ionic Liquid 1-Ethyl-3-Methylimidazolium Ethylsulfate Using X-Ray Photoelectron Spectroscopy (XPS). *Z. Phys. Chem.* **2006**, *220*, 1439−1453.
(40) Hunger, J.; Stoppa, A.; Buchner, R.; G, H. Dipole Correlations in the Ionic Liquids 1-N-Ethyl-3-N-methylimidazolium Ethylsulfate and Its Binary Mextures with Dichoromethane. *J. Phys. Chem. B* **2009**, *113*, 9527−9537.
(41) Pronk, S.; Páll, S.; Schulz, R.; Larsson, P.; Bjelkmar, P.; Apostolov, R.; Shirts, M. R.; Smith, J. C.; Kasson, P. M.; van der Spoel, D.; et al. GROMACS 4.5: A High-Throughput and Highly Parallel Open Source Molecular Simulation Toolkit. *Bioinformatics* **2013**, *29*, 845−854.
(42) Jorgensen, W. L.; Maxwell, D. S.; Tirado-Rives, J. Development and Testing of the OPLS All-Atom Force Field on Conformational Energetics and Properties of Organic Liquids. *J. Am. Chem. Soc.* **1996**, *118*, 11225−11236.

DOI: 10.1021/acs.jpcb.7b00160
J. Phys. Chem. B 2017, 121, 4845−4852

(43) Canongia Lopes, J. N.; Pádua, A. Molecular Force Field for Ionic Liquids III: Imidazolium, Pyridinium, and Phosphonium Cations; Chloride, Bromide, and Dicyanamide Anions. *J. Phys. Chem. B* **2006**, *110*, 19586−19592.
(44) Canongia Lopes, J. N.; Pádua, A.; Shimizu, K. Molecular Force Field for Ionic Liquids IV: Trialkylimidazolium and Alkoxycarbonyl-Imidazolium Cations; Alkylsulfonate and Alkylsulfate Anions. *J. Phys. Chem. B* **2008**, *112*, 5039−5046.
(45) Yan, T.; Burnham, C. J.; Del Pópolo, M. G.; Voth, G. A. Molecular Dynamics Simulation of Ionic Liquids: The Effect of Electronic Polarizability. *J. Phys. Chem. B* **2004**, *108*, 11877−11881.
(46) Borodin, O. Polarizable Force Field Development and Molecular Dynamics Simulations of Ionic Liquids. *J. Phys. Chem. B* **2009**, *113*, 11463−11478.
(47) Schröder, C.; Sonnleitner, T.; Buchner, R.; Steinhauser, O. The influence of polarizability on the dielectric spectrum of the ionic liquid 1-ethyl-3-methylimidazolium triflate. *Phys. Chem. Chem. Phys.* **2011**, *13*, 12240−12248.
(48) Schröder, C.; Steinhauser, O. The influence of electrostatic forces on the structure and dynamics of molecular ionic liquids. *J. Chem. Phys.* **2008**, *128*, 224503−7.
(49) Schröder, C.; Steinhauser, O. Using fit functions in computational dielectric spectroscopy. *J. Chem. Phys.* **2010**, *132*, 244109−16.
(50) Yamamoto, K.; Tani, M.; Hangyo, M. Terahertz Time-Domain Spectroscopy of Imidaznolium Ionic Liquids. *J. Phys. Chem. B* **2007**, *111*, 4854−4859.
(51) Bursulaya, B. D.; Kim, H. J. Spectroscopic and dielectric properties of liquid water: A molecular dynamics simulation study. *J. Chem. Phys.* **1998**, *109*, 4911−4919.
(52) Gonzalez-Jimenez, M.; Ramakrishnan, G.; Harwood, T.; Lapthorn, A. J.; Kelly, S. M.; Ellis, E. M.; Wynne, K. Observation of coherent delocalized phonon-like modes in DNA under physiological conditions. *Nat. Commun.* **2016**, *7*, 11799.
(53) Turton, D. A.; Senn, H. M.; Harwood, T.; Lapthorn, A. J.; Ellis, E. M.; Wynne, K. Terahertz underdamped vibrational motion governs protein-ligand binding in solution. *Nature Commun.* **2014**, *5*, 3999.
(54) Wu, E. C.; Kim, H. J. MD Study of Stokes Shifts in Ionic Liquids: Temperature Dependence. *J. Phys. Chem. B* **2016**, *120*, 4644−4653.
(55) Wulf, A.; Fumino, K.; Ludwig, R.; Taday, P. Combined THz, FIR and Raman Spectroscopy Studies of Imidazolium-Based Ionic Liquids Covering the Frequency Range 2−300 cm^{-1}. *ChemPhysChem* **2010**, *11*, 349−353.

DOI: 10.1021/acs.jpcb.7b00160
J. Phys. Chem. B 2017, 121, 4845−4852